Slip and no-slip velocity boundary conditions at interface of porous, plain media

M. SAHRAOUI and M. KAVIANY

Department of Mechanical Engineering and Applied Mechanics,
The University of Michigan, Ann Arbor, MI 48109, U.S.A.

Abstract—The hydrodynamic boundary condition at the interface between a porous and a plain medium is examined by direct simulation of the two-dimensional flow field near the interface of a porous medium made of cylinders. The existing slip boundary condition, which contains a slip coefficient α, and the no-slip boundary condition, which contains an effective viscosity μ′, are examined. The dependence of α on the direction of the flow (with respect to the interfacial plane), the porosity, the Reynolds number (based on the unit cell length and the Darcean velocity), the selection of the interfacial location, and the arrangement of the cylinders (structure) is examined in detail. The numerical results show that α is not only a function of the structure but also depends on the flow direction, the Reynolds number, the extent of the plain medium, and the nonuniformities in the arrangement of the surface particles. It is also shown that for an accurate prediction of the local velocity near the interface (inside the porous medium), μ′ must vary within the porous medium. This shows that the Brinkman extension based on a uniform μ′, and the associated screening distance, do not satisfactorily model the flow field in the porous medium.

1. INTRODUCTION

FOR FLOW through a porous medium bounded on one of its boundaries by a plain medium, special attention must be given to the hydrodynamic boundary condition at this porous, plain medium interface. The flow in the porous medium is governed by the empirical Darcy law (for creeping flows), i.e.

$$-\frac{\mu}{K}\mathbf{u}_{\mathrm{D}} = \nabla\langle p\rangle_V^f \qquad (1)$$

where μ is the local fluid viscosity, K the local isotropic permeability of the porous medium, $\mathbf{u}_{\mathrm{D}}$ the Darcean velocity vector, and $\langle p\rangle_V^f$ the fluid phase (or pore) averaged pressure. The Darcean velocity is a volume (fluid and solid phases) averaged velocity for a local representative elementary volume located away from the interface, i.e.

$$\mathbf{u}_{\mathrm{D}} = \langle\mathbf{u}\rangle_V(y \to -\infty) \qquad (2)$$

where the origin of y is taken at the porous, plain medium interface. The averages used in equations (1) and (2) will be defined in Section 4. When the permeability of the porous medium is very small, i.e. the velocity in the stationary porous medium is much smaller than the average velocity in the plain medium, a zero velocity at this interface is assumed. As the flow within the porous medium becomes significant, the non-zero interfacial velocity is generally estimated using the empirical boundary condition of Beavers and Joseph [1], which introduces a slip coefficient α. Another approach is the application of the no-slip condition formulated by Brinkman [2], which introduces an 'effective' viscosity μ′.

In the slip boundary condition, the interfacial shear

is related to the slip velocity at the interface through

$$\left.\frac{\mathrm{d}\langle u\rangle_A}{\mathrm{d}y}\right|_{y=0^+} = \frac{\alpha}{K^{1/2}}(\langle u\rangle_{A,\mathrm{i}} - u_{\mathrm{D}}) \qquad (3)$$

where α is the slip coefficient, $y = 0^+$ indicates that the velocity gradient is evaluated at the interface and towards the plain medium, $\langle u\rangle_A$ denotes the area averaged velocity component along x, $\langle u\rangle_{A,\mathrm{i}}$ is the area averaged slip (interface) velocity evaluated at $y = 0$, u_{D} is the component along x of $\mathbf{u}_{\mathrm{D}}$ defined by equation (1) and K is the permeability. In the Beavers and Joseph experiments, a one-dimensional Poiseuille flow is realized through a channel of width h bounded by a porous medium at $y = 0$ on the one side, and an impermeable surface at $y = h$ on the other side. The flow in the channel is governed by

$$-\frac{\mathrm{d}p}{\mathrm{d}x} + \mu\frac{\mathrm{d}^2 u}{\mathrm{d}y^2} = 0 \qquad (4)$$

and for the porous medium, they assumed a uniform Darcean velocity u_{D}. For this one-dimensional problem, we require at the interface that

$$\langle p\rangle_V^f = p \quad \text{and} \quad \frac{\mathrm{d}\langle p\rangle_V^f}{\mathrm{d}x} = \frac{\mathrm{d}p}{\mathrm{d}x}. \qquad (5)$$

Using the slip boundary condition at the interface ($y = 0$), and the no-slip boundary condition at the impermeable surface of the channel ($y = h$), the velocity distribution is

$$u(y) = \langle u\rangle_{A,\mathrm{i}}\left(1 + \frac{\alpha}{K^{1/2}}y\right) + \frac{1}{2\mu}(y^2 + 2\alpha y K^{1/2})\frac{\mathrm{d}p}{\mathrm{d}x} \qquad (6)$$

NOMENCLATURE

C proportionality constant for the suction velocity

d cylinder diameter [m]

h channel size [m]

K bulk permeability [m^2]

$K(y)$ local permeability [m^2]

l cell dimension [m]

$\dot{m}_c$ mass flow rate per unit depth through the channel [kg m^{-1} s^{-1}]

$(\dot{m}_x/\rho)(x = 0)$ volumetric flow rate per unit depth at $x = 0$,
$(\dot{m}_x/\rho)(x = 0) = \int_{y_1}^{h} u(0, y)\, dy$ [m^2 s^{-1}]

$(\dot{m}_x/\rho)(x = l)$ volumetric flow rate per unit depth at $x = l$,
$(\dot{m}_x/\rho)(x = l) = \int_{y_1}^{h} u(l, y)\, dy$ [m^2 s^{-1}]

$\dot{m}_y/\rho$ volumetric flow rate per unit depth from upper and lower boundaries,
$\dot{m}_y/\rho = \int_0^l (v(x, y_1) - v(x, h))\, dx$ [m^2 s^{-1}]

p pressure [N m^{-2}]

p^* dimensionless pressure, $p/(\rho u_D^2)$

p_p average pressure for plain medium [N m^{-2}]

$\langle p \rangle^f$ cell averaged pressure taken over fluid volume [N m^{-2}]

Δp pressure difference applied across the cell [N m^{-2}]

r radial coordinate [m]

Re_l Reynolds number based on the Darcy velocity, $u_D l/\nu$

S_r source term in the radial component of the momentum equation

S_θ source term in the tangential component of the momentum equation

t time [s]

t^* dimensionless time, $t u_D/l$

u velocity in the x-direction [m s^{-1}]

u^* dimensionless velocity in the x-direction, u/u_D

u_D Darcy velocity [m s^{-1}]

$\langle u \rangle_A$ area averaged velocity [m s^{-1}]

$\langle u \rangle_V$ volume averaged velocity [m s^{-1}]

$\langle u_i \rangle_A$ area averaged interface velocity [m s^{-1}]

v velocity in the y-direction [m s^{-1}]

v^* dimensionless velocity in the y-direction

V_0 blowing velocity [m s^{-1}]

$\mathbf{x}$ position vector [m]

x, y Cartesian coordinates [m]

x_0, y_0 reference point for stream function [m]

x^*, y^* dimensionless Cartesian coordinates, x/l and y/l

y_i distance from the nominal interface where the boundary condition is applied

y_1 lower boundary of the computational domain.

Greek symbols

α slip coefficient

$\delta_1, \delta_2, \delta_3$ arrangement parameters for the bed of cylinders [m]

ε porosity

θ tangential coordinate

λ offset in the y-direction between two adjacent interfacial cylinders, for in-line arrangement [m]

μ dynamic viscosity [kg m^{-1} s^{-1}]

μ' Brinkman effective viscosity [kg m^{-1} s^{-1}]

$\mu'(y)$ variable effective viscosity [kg m^{-1} s^{-1}]

ν kinematic viscosity [m^2 s^{-1}]

ξ position vector [m]

ρ density [kg m^{-3}]

σ $h/K^{1/2}$

$\psi(x, y)$ stream function [m^2 s^{-1}]

$\Delta\psi$ stream function increment [m^2 s^{-1}].

Subscripts

A area

D Darcy

i interfacial

l at $x = l$

p plain medium

r radial direction

T total

V volume

x x-direction

y y-direction

θ tangential direction

$+$ plain medium side

$-$ porous medium side.

Superscripts

$*$ dimensionless

f fluid.

Other symbols

$\langle\ \rangle_A$ area averaged

$\langle\ \rangle_V$ volume averaged

$O(\ )$ order of magnitude.

where the slip velocity $\langle u \rangle_{A,i}$ is given by

$$\langle u \rangle_{A,i} = -\frac{K}{2\mu}\left(\frac{\sigma^2 + 2\alpha\sigma}{1 + \alpha\sigma}\right)\frac{dp}{dx} \qquad (7)$$

by using $\sigma = h/K^{1/2}$. The mass flow rate through the channel per unit depth becomes

$$\dot{m}_c = -\frac{\rho h^3}{12\mu}\frac{dp}{dx} - \frac{\rho h^3}{4\mu\sigma}\left(\frac{\sigma + 2\alpha}{1 + \alpha\sigma}\right)\frac{dp}{dx} \qquad (8)$$

where ρ is the fluid density. Experimental evidence of the validity of the proposed boundary condition was presented in refs. [1, 3, 4], by varying the channel size while keeping the pressure gradient constant. It was shown that for a given porous medium, a constant α is needed to correlate the mass flow rate $\dot{m}_c$ for all the gap sizes considered. In the experiments, various porous media (different permeabilities and structures) were used and α ranged from 0.1 to 4.0.

The slip boundary condition has been theoretically examined by Saffman [5], where he used a statistical approach to postulate a generalized Darcy law for flow in non-homogeneous porous media. According to his formulation, the flow through the porous medium is given by

$$\mu \int k_{ij}(\mathbf{x}, \xi)\langle v_j \rangle_V(\xi)\,d\xi = \frac{\mu}{\varepsilon}\nabla^2\langle v_i \rangle_V - \frac{\partial\langle p \rangle_V^f}{\partial x_i} \qquad (9)$$

where $\langle v_i \rangle_V$ denotes the volume averaged component of the velocity vector, $k_{ij}(\mathbf{x}, \xi)$ the flow resistance kernel, and $\mathbf{x}$ and ξ are position vectors. The vector $\mathbf{x}$ indicates the position where the resistance is being evaluated and ξ indicates the points contributing to this resistance. The Darcy law, given by equation (1), is a first-order approximation of this generalized equation (9), i.e.

$$k_{ij}(\mathbf{x}, \xi) \to \frac{\delta_{ij}}{K}\delta(\mathbf{x} - \xi)$$

where δ is the Dirac delta and δ_{ij} is the Kronecker delta. At the interface, this first-order approximation of the kernel is not valid, and other terms of the expansion (with higher derivatives of the delta function) have to be included. Saffman considered a one-dimensional model, governed by equation (4) in the plain medium. He used equation (9) for the porous medium and normalized this equation with $K^{1/2}$ and $(\mu/K)\,d\langle p \rangle_V^f/dx$, as the length and the velocity scales. He obtained a general, asymptotic solution for flow near the interface, and with an order of magnitude analysis, based on the screening distance $K^{1/2}$, he arrived at the boundary condition

$$\langle u \rangle_{A,i} = \frac{K^{1/2}}{\alpha}\frac{\partial\langle u \rangle_A}{\partial n} + O(K) \qquad (10)$$

where n denotes the normal to the interface. He also found that α depends strongly on the position and

decreases noticeably over a distance of the order of $K^{1/2}$, a result confirmed by the present investigation.

An experimental and an analytical investigation of this interfacial hydrodynamic boundary condition were conducted [6, 7]. The model used in this investigation consisted of a grooved plate, separated by a gap from a moving parallel plate (resulting in a Couette flow through the gap and in the grooves). The experimental results [6] showed that for gap sizes larger than half of the spacing between two adjacent grooves, α reaches an asymptote (becoming independent of the gap size). The analytical study [7] showed that α increases as the permeability decreases. This result contradicts the experimental results [1] for real porous media, where it has been shown that α increases with an increase in the permeability. The discrepancy is due to the idealization of the actual inter-connected pores by a grooved plate.

Larson and Higdon [8, 9] considered a more realistic model, i.e. the Stokes flow through a semi-infinite, periodic structure (two-dimensional) made of cylinders, with flow either parallel or perpendicular to the cylinder axes. The boundary integral method was used to solve the Stokes equation for flow around different arrangements of cylinders (square and hexagonal arrangements). When the flow was perpendicular to the cylinder axes and parallel to the interfacial plane, they obtained slip velocities which were in the direction opposite to the velocity in the plain and the porous medium for $\varepsilon < 0.9$. This nonphysical result is due to their choice of the interfacial location. Their slip velocity was calculated using the volumetric flow rate above the interface (for shear flows), i.e.

$$\frac{\dot{m}_c}{\rho} = \langle u \rangle_{A,i}h + \tfrac{1}{2}\gamma h^2 \qquad (11)$$

where γ is the applied velocity gradient at the impermeable boundary of the channel ($y = h$). In their calculation of the slip velocity, the interfacial location was chosen to be the plane passing through the axes of the interfacial row of cylinders. However, the plain medium flow occurs above the surface tangent to the top of the interfacial cylinders. The contribution to $\dot{m}_c$, of the flow between this surface and their defined interface, is small for $\varepsilon < 0.9$. This is due to the vortices present between adjacent cylinders. Due to this over-estimation of h, a slip velocity opposing the direction of the plain medium flow, is obtained using equation (11). They state that due to the ambiguity in the definition of the interfacial location, any reasonable value for α can be correct.

In the no-slip boundary condition, the interface is treated as a part of a continuum. In this approach, as formulated by Brinkman, a macroscopic shear term is added to the Darcy law, to account for the velocity gradient present at the interface. With the addition of this shear term, equation (1) becomes

$$-\frac{\mu}{K}\langle \mathbf{u} \rangle_V + \mu'\nabla^2\langle \mathbf{u} \rangle_V = \nabla\langle p \rangle_V^f \qquad (12)$$

where μ' is the effective viscosity and is presumed constant in the original Brinkman model. This will guarantee the continuity of the velocity and the shear, at the interface. The one-dimensional solution (for a Poiseuille flow) of the Brinkman equation was compared in ref. [10] to that based on the Beavers and Joseph slip boundary condition, given by equation (6), and it was found that for this flow $\mu'/\mu = \alpha^2$. This model has been used in ref. [11] to treat a jump in the permeability across the interface with the addition of a velocity-squared term (bulk inertia effect) to the Darcy equation. This bulk inertia term does not unveil the effect of the flow inertia on the pore level hydrodynamics especially at the interface where it is more important than away from the interface.

As will be shown, the effective viscosity μ', when treated as being uniform throughout the porous medium (including the interface), does not lead to an accurate prediction of the velocity distribution near the interface. When allowance is made for the variation of μ' with y, we have for one-dimensional flow

$$-\frac{\mu}{K}\langle u\rangle_v + \frac{d}{dy}\left[\mu'(y)\frac{d\langle u\rangle_v}{dy}\right] = \frac{d\langle p\rangle_v^f}{dx} \quad (13)$$

where $\mu'(y)$ is the variable effective viscosity which accounts for the presence of the interface. The presence of the interface could also be modeled through the permeability variation, i.e.

$$-\frac{\mu}{K(y)}\langle u\rangle_v + \mu'\frac{d^2\langle u\rangle_v}{dy^2} = \frac{d\langle p\rangle_v^f}{dx}. \quad (14)$$

This model has been used in refs. [12, 13] to predict the momentum and heat transfer at impermeable surfaces bounding packed beds. Sangani and Behl [14] used a combination of the variable permeability and viscosity models (i.e. a combination of equations (13) and (14)) to solve for a shear flow over a porous medium made of spheres. They used the void distribution of their bed of spheres to model the variations in the local permeability and viscosity. They assumed inverse and direct proportionality between the local K and μ' and the local planar void fraction, respectively. Their predicted interfacial velocity was in good agreement with the results from their local simulation. It should be mentioned that if such arbitrary relationships for the local K and μ' are not assumed, then the simultaneous determination of these relations, using the results from local simulation, is not possible. A more detailed review of the slip and no-slip boundary conditions can be found in ref. [15].

In this study, the flow at the interface between porous and plain media is investigated by the direct simulation of the flow in a porous medium made of cylinders. Unlike the previous studies, the full Navier–Stokes equation is solved, enabling us to study the inertial effect which exits at the interface (even for cases where the flow in the porous medium, away from the interface, is Darcean). Also, previous studies of the interface have been on parallel flows (Poiseuille,

or Couette) and flows oblique to the interface have not been studied. This has resulted in an ambiguity in the role and the significance of a second shear stress term arising from the normal velocity. In this study, parallel and oblique flows are studied in order to examine the effect of the two-dimensionality of the flow on α. Also, in contrast to the previous studies, α is computed using the local velocity and the local velocity gradient (instead of $\dot{m}_c$). In the experimental investigation [4], it was established that the surface structure (in contrast to the bulk structure), also influences α significantly. In this study, structural non-uniformities (at the surface) are considered, and it is shown that α changes appreciably with these non-uniformities. Thus, establishing the dominance of the surface hydrodynamics over the bulk.

The no-slip condition and the associated variable K and μ', are also examined in order to determine their variations near the interface.

2. ANALYSIS

For a better understanding of the slip and no-slip boundary conditions, a direct (point-wise) simulation of the flow around the interface is performed. The Navier–Stokes equation is solved for a porous medium made of cylinders, as shown in Fig. 1(a). The arrangement shown is a general one for mono-sized cylinders. Figure 1(b) shows the arrangement at the interface, and shows the nominal location of the interface ($y = 0$), which is taken to be at the top of the interfacial cylinders. Different arrangements of cylinders are obtained by selection of the distances δ_1, δ_2, and δ_3 shown in Fig. 1(a). In this study, both in-line and staggered arrangements of cylinders are studied. In these simple periodic structures, the flow field far away from the interface (i.e. bulk behavior) is determined by obtaining the point solution for a unit cell which generally contains only one particle (cylinder). This is shown in Figs. 1(c) and (d). When the flow near the interface is simulated, the domain under study includes the plain medium as well as several cylinders, as shown in Fig. 1(b), depending on the particular arrangement considered.

The two-dimensional momentum and continuity equations are solved by discretization using the finite-difference approximations. Since the boundary of the unit cell and the computation domain are planar, a cylindrical–Cartesian grid over-laying scheme is used. A bilinear interpolation is used to communicate between the two coordinates. This method has been successfully used in ref. [16] to predict the flow and heat transfer in tube banks and in ref. [17] to predict forced convection evaporation from a curved cavity.

The momentum and continuity equations are solved for the dimensionless, primitive variables, u^*, v^*, and p^*, in each of the coordinate systems. In the Cartesian coordinates, the dimensionless continuity and momentum equations, for laminar, incompressible flows are

$$\frac{\partial u^*}{\partial x^*} + \frac{\partial v^*}{\partial y^*} = 0 \qquad (15)$$

$$\frac{\partial u^*}{\partial t^*} + u^* \frac{\partial u^*}{\partial x^*} + v^* \frac{\partial u^*}{\partial y^*} = -\frac{\partial p^*}{\partial x^*}$$

$$+ \frac{1}{Re_l}\left(\frac{\partial^2 u^*}{\partial x^{*2}} + \frac{\partial^2 u^*}{\partial y^{*2}}\right) \qquad (16)$$

$$\frac{\partial v^*}{\partial t^*} + u^* \frac{\partial v^*}{\partial x^*} + v^* \frac{\partial v^*}{\partial y^*} = -\frac{\partial p^*}{\partial y^*}$$

$$+ \frac{1}{Re_l}\left(\frac{\partial^2 v^*}{\partial x^{*2}} + \frac{\partial^2 v^*}{\partial y^{*2}}\right) \qquad (17)$$

where the scaling is done using u_D for the velocity scale, l (unit cell length) for the length, and l/u_D for

the time. The particle Reynolds number Re_l is $u_D l/v$. In the porous medium and far from the interface, the bulk (i.e. not affected by the interface) flow behavior is observed, and the periodic boundary conditions can be applied to the unit cell. These periodic boundary conditions are given in Figs. 1(c) and (d) for in-line and staggered arrangements. The flow is driven by the prescribed pressure gradient Δp^*. The pressure gradient and the particle Reynolds number are not known a priori, because the volume averaged velocity u_D is not known. Thus, an arbitrary pressure gradient and Reynolds number are assigned. Then, the actual pressure gradient and Reynolds number are obtained by re-scaling, using the computed volume averaged velocity. For Couette flows, the flow is driven by the impermeable boundary of the channel ($y = h$). Since
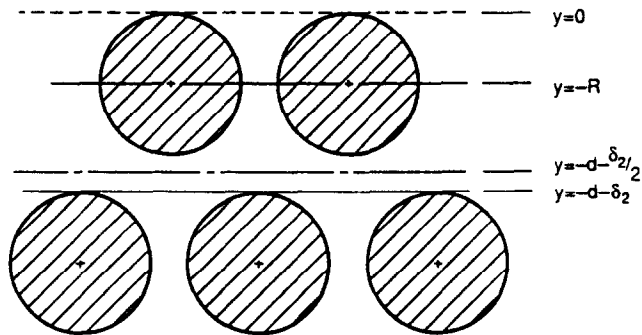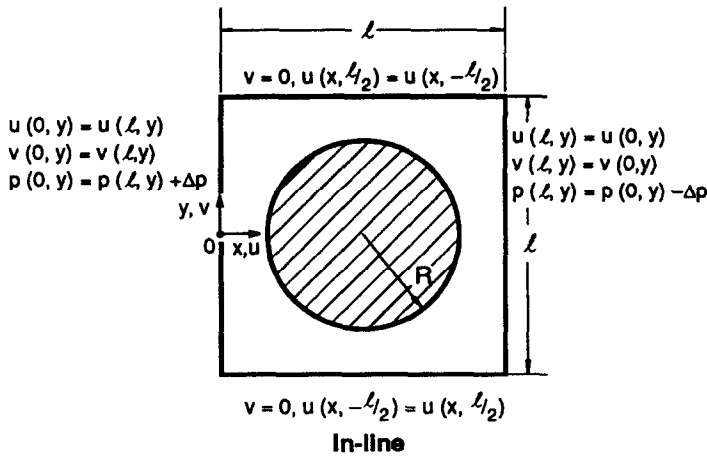
(a)
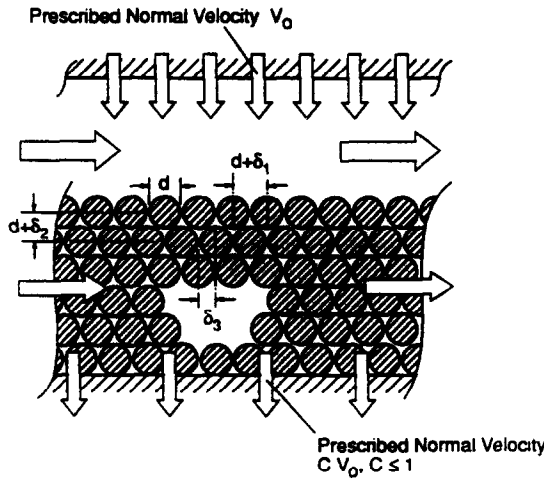
(b)

Fig. 1. (a) Generalized arrangement of mono-sized cylinders used to model the interface between plain and porous media, (b) location of $y = 0$ (nominal interface), (c) and (d) periodic boundary conditions for a unit cell in the porous medium, for in-line and staggered arrangements, respectively.

(c)

v = 0, u (x, $^\ell/_2$) = u (x, $-^\ell/_2$)

u (0, y) = u (ℓ, y)
v (0, y) = v (ℓ,y)
p (0, y) = p (ℓ, y) +Δp

u (ℓ, y) = u (0, y)
v (ℓ, y) = v (0,y)
p (ℓ, y) = p (0, y) −Δp

v = 0, u (x, $-^\ell/_2$) = u (x, $^\ell/_2$)

In-line

(d)

v = 0, u (x, $^\ell/_2$) = u (x, $-^\ell/_2$)

u (0, y) = u (ℓ,y')
v (0, y) = v (ℓ,y')
p (0, y) = p (ℓ,y') +Δp

u (ℓ, y) = u (0,y')
v (ℓ, y) = v (0,y')
p (ℓ, y) = p (0,y') −Δp

v = 0, u (x, $-^\ell/_2$) = u (x, $^\ell/_2$)

Staggered

$$y' = -^\ell/_2 + y; \quad y \geq 0$$
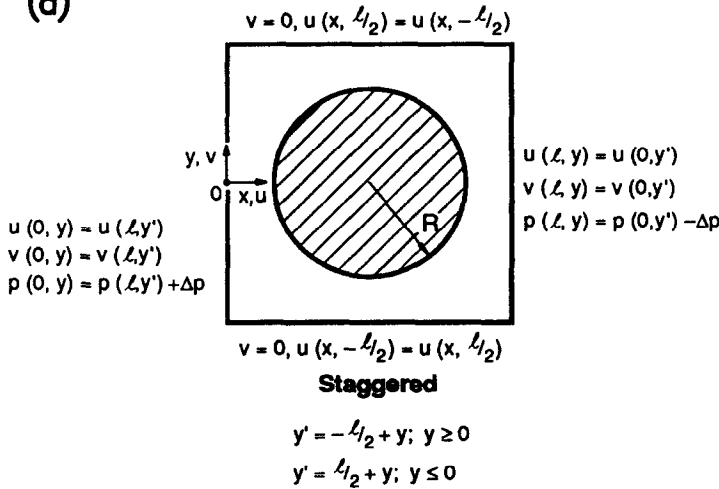$$y' = ^\ell/_2 + y; \quad y \leq 0$$

FIG. 1.—*continued.*

no pressure gradient is applied, the volume averaged velocity u_D is zero. Thus for this case, the velocity at the impermeable boundary is used for the scaling.

Whenever the plain medium is included in the computational domain, the no-slip boundary condition is applied at the impermeable channel wall. For oblique flows (Fig. 1(a)), the left- and right-hand side boundaries are treated differently to account for the lateral volumetric flow into the control volume (from the upper and lower boundaries), i.e.

$$\frac{\dot{m}_y}{\rho} = \int_0^l [v(x,y_1) - v(x,h)]\,\mathrm{d}x$$

where y_1 is the lower boundary and where $v(x, y_1)$ and $v(x, h)$ are the prescribed velocities at the lower and upper boundaries of the computational domain. For the right boundary ($x = l$) and for a given y, the

velocity $u(l, y)$ is equal to the inlet velocity $u(0, y)$ plus a fraction of the lateral volumetric flow. This fraction is determined by the ratio of $u(0, y)$ to the total inlet volumetric flow, i.e.

$$\frac{\dot{m}_x}{\rho}(x = 0) = \int_{y_1}^h u(0,y)\,\mathrm{d}y.$$

Then, the boundary condition becomes

$$u(l,y) = u(0,y) + \frac{u(0,y)}{\dfrac{\dot{m}_x}{\rho}(x=0)}\left(\frac{\dot{m}_y}{\rho}\right)$$

similarly, at $x = l$

$$\frac{\dot{m}_x}{\rho}(x = l) = \int_{y_1}^h u(l,y)\,\mathrm{d}y$$

and

$$u(0, y) = u(l, y) - \frac{u(l, y)}{\dfrac{\dot{m}_x}{\rho}(x = l)} \left(\frac{\dot{m}_y}{\rho} \right).$$

The boundary condition for the v component for oblique flows is periodic (similar to the parallel flows) at $x = 0$ and l.

For the cylindrical coordinates, the dimensionless continuity and momentum equations are

$$\frac{\partial r^* v_r^*}{\partial r^*} + \frac{\partial v_\theta^*}{\partial \theta} = 0 \tag{18}$$

$$\frac{\partial v_r^*}{\partial t^*} + v_r^* \frac{\partial v_r^*}{\partial r^*} + \frac{v_\theta^*}{r^*} \frac{\partial v_r^*}{\partial \theta} = -\frac{\partial p^*}{\partial r^*} + \frac{1}{Re_l}$$

$$\times \left[\frac{1}{r^*} \frac{\partial}{\partial r^*} \left(r^* \frac{\partial v_r^*}{\partial r^*} \right) + \frac{1}{r^*} \frac{\partial}{\partial \theta} \left(\frac{1}{r^*} \frac{\partial v_r^*}{\partial \theta} \right) \right] + S_r \tag{19}$$

$$\frac{\partial v_\theta^*}{\partial t^*} + v_r^* \frac{\partial v_\theta^*}{\partial r^*} + \frac{v_\theta^*}{r^*} \frac{\partial v_\theta^*}{\partial \theta} = -\frac{1}{r^*} \frac{\partial p^*}{\partial \theta} + \frac{1}{Re_l}$$

$$\times \left[\frac{1}{r^*} \frac{\partial}{\partial r^*} \left(r^* \frac{\partial v_\theta^*}{\partial r^*} \right) + \frac{1}{r^*} \frac{\partial}{\partial \theta} \left(\frac{1}{r^*} \frac{\partial v_\theta^*}{\partial \theta} \right) \right] + S_\theta \tag{20}$$

where the source terms S_r and S_θ are

$$S_r = \frac{1}{Re_l} \left\{ -2 \frac{v_r^*}{r^{*2}} + \frac{2}{r^{*2}} \frac{\partial v_\theta^*}{\partial \theta} + \frac{1}{r^*} \frac{\partial}{\partial r^*} \left(r^* \frac{\partial v_r^*}{\partial r^*} \right) \right.$$

$$\left. + \frac{\partial}{\partial \theta} \left[\frac{\partial}{\partial r^*} \left(\frac{v_\theta^*}{r^*} \right) \right] \right\} + \frac{v_\theta^{*2}}{r^*} \tag{21}$$

$$S_\theta = \frac{1}{Re_l} \left(-\frac{v_\theta^*}{r^{*2}} + \frac{2}{r^{*2}} \frac{\partial v_r^*}{\partial \theta} \right) - \frac{v_r^* v_\theta^*}{r^*} \tag{22}$$

and the boundary conditions are $v_r^* = v_\theta^* = 0$ at $r^* = d/2l$.

3. SOLUTION METHOD

The equations are discretized by integrating the above equations over a finite control volume. The discretized equations are solved using the pressure correction method as described by Patankar [18]. The power-law scheme is used to evaluate the fluxes at the control volume faces.

As mentioned previously, iterations are performed alternatively in the two grid nets, and the values of the unknown at the boundaries of these grid nets are obtained using the bilinear interpolation. This bilinear interpolation is performed in the overlaying region, which extends 3–4 grid nodes. An unknown variable on the boundary of the cylindrical grid net is obtained by the bilinear interpolation, using the four surrounding nodes in the Cartesian grid. The same procedure is used for a variable on the boundary of the Cartesian grid net. In order to solve for u^*, v^*, and p^* fields, five iterations are done in the Cartesian domain. The bilinear interpolation is then used to find the boundary conditions for the cylindrical domain, where the next five iterations are performed. After

these iterations, interpolations are made back to the Cartesian grid (for every cylinder in the domain). More detail about the numerical technique is available in ref. [17].

For most of the simulations, only one cylinder is needed, since the numerical experiments show that the bulk flow behavior is approached at the lower half of the first row of cylinders (i.e. the interfacial cylinders). More cylinders are needed for the staggered arrangements, since the interfacial effect penetrates much further into the porous medium. Also for the staggered arrangements, two columns of cylinders are used because the boundary conditions shown in Fig. 1(d) cannot be used. Figures 2(a)–(c) show some examples of the constant stream function contours for different flow types and arrangements. They also show the typical domains used in the computations. The stream function is obtained by integrating the velocity field, i.e.

$$\psi(x, y) = -\int_{x_0}^{x} v(\zeta, y_0) \, d\zeta + \int_{y_0}^{y} u(x, \zeta) \, d\zeta \tag{23}$$

where (x_0, y_0) is a reference point with a prescribed value of zero for the stream function. In Fig. 2(a), this point is taken at the center of the cylinder at the lower boundary of the domain. For Figs. 2(b) and (c), it is taken at the center of the only cylinder used. Note that near the interface unequal increments of the stream function are used due to the higher velocities. Both Figs. 2(a) and (b) are for Poiseuille flows and Fig. 2(c) is for an oblique flow. The penetration of the interfacial effect for the staggered arrangement is clearly shown in Fig. 2(a), where flow becomes symmetric after the third row of cylinders. Note that for the staggered arrangement shown in Fig. 2(a), the cylinders are in-line in the y-direction which results in an anisotropic packed bed.

In order to test the accuracy of the finite-difference scheme and the bilinear interpolation, grid accuracy tests were performed. In this test, the grid size dependence was tested. For example, by doubling the number of grid points (in each direction) from 100×100 to 200×200, a 0.01% difference in the volume averaged velocity u_D is obtained for $Re_l = 1$ and $\Delta p^* = 660$ for the in-line arrangement. The same test was performed for $Re_l = 150$ and $\Delta p^* = 5.3$, and a 1% difference in u_D was found. This convergence test establishes the accuracy of the numerical scheme, particularly the bilinear interpolation.

The computed results are also compared to the available experimental results. Figure 2(d) shows the dimensionless pressure drop as a function of the Reynolds number for flow over in-line cylinders from experiments for isothermal flows of oil over a bank of in-line tubes [19]. The difference between the numerical and experimental results is within 10 and 20%, for low and high Reynolds numbers, respectively. This discrepancy can be due to some experimental limitations such as the finiteness of the bed, where the end
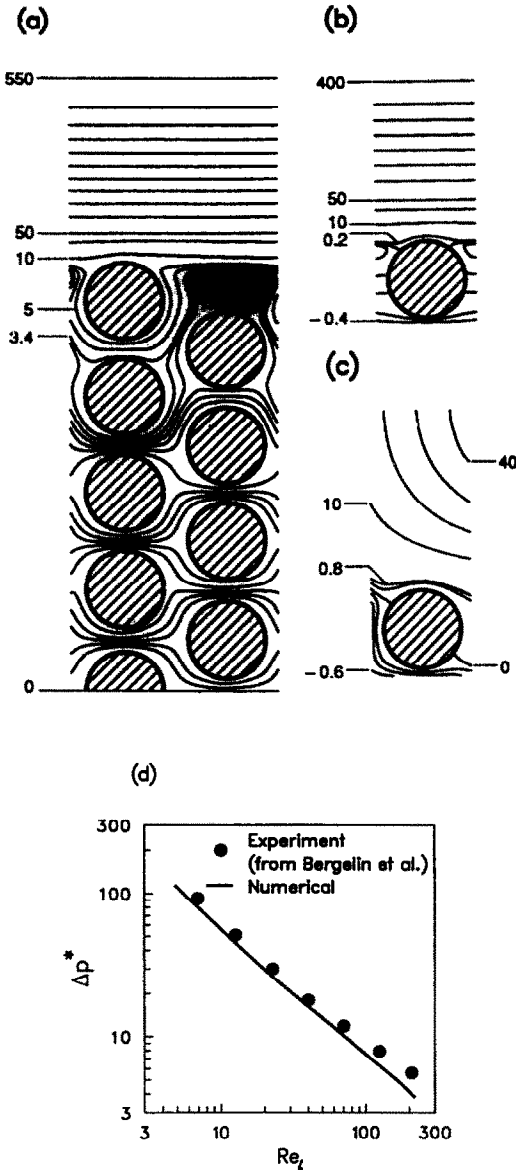
(a) **(b)**

(c)

(d)

FIG. 2. Stream function contours for different interfacial flows. (a) Poiseuille flow for staggered arrangement $\psi = 0.2$–3.4 ($\Delta\psi = 0.2$); 4.25; 10–50 ($\Delta\psi = 20$); 50–550 ($\Delta\psi = 50$), (b) Poiseuille flow for in-line arrangement $\psi = -0.4$–0.2 ($\Delta\psi = 0.2$); 10–50 ($\Delta\psi = 20$); 50–400 ($\Delta\psi = 50$), and (c) oblique flow for in-line arrangement $\psi = -0.6$–0 ($\Delta\psi = 0.2$); 0–0.8 ($\Delta\psi = 0.4$); 10–40 ($\Delta\psi = 10$). (d) Comparison of the numerical and experimental pressure drop across in-line packed bed of cylinders, as a function of the Reynolds number (for $\varepsilon = 0.497$).

effects may influence Δp. The numerical results were also compared with the finite-element results on computed permeability for various arrangements (available in ref. [20]) and a 2% agreement is obtained.

4. RESULTS FOR SLIP CONDITION

The point variation of the velocity and pressure are obtained by solving the point conservation equations

(15)–(20) along with the prescribed boundary conditions. In order to relate these point (pore-level or micro) variations to the macro or the Darcean behavior, area and volume averages must be taken. The area average is defined as (for example for u)

$$\langle u \rangle_A(y) \equiv \frac{1}{l} \int_0^l u(x, y) \, dx. \tag{24}$$

The interfacial, tangential velocity $\langle u \rangle_{A,i}$ is defined as

$$\langle u \rangle_{A,i} = \langle u \rangle_A(y_i) \tag{25}$$

where y_i is the selected interfacial location. The volume average for a cell, as shown in Figs. 1(c) and (d), is defined as

$$\langle u \rangle_V(y) \equiv \frac{1}{l^2} \int_0^l \int_{-l/2}^{l/2} u(x, y+\zeta) \, d\zeta \, dx. \tag{26}$$

The pressure is averaged on the fluid phase only, i.e.

$$\langle p \rangle_V^f = \frac{1}{V_f} \int_{V_f} p \, dV. \tag{27}$$

Later in the discussion of the no-slip condition, we will introduce a volume averaging that uses a variable volume size.

4.1. Interface position

A major difficulty associated with the Beavers and Joseph boundary condition is the choice of the interfacial location, where the boundary condition is applied. Beavers and Joseph suggested the tangent to the surface of the outermost pore as the interface. For the arrangement of cylinders considered here, this would be the tangent to the top of the interfacial layer of cylinders, which we have defined as the nominal interface and assigned as the origin of the y-axis as shown in Fig. 1(b).

Because the interfacial effects generally penetrate in the porous medium over distances of the order of the Brinkman screening distance $K^{1/2}$, we need to examine the magnitude of this distance for a bed of cylinders. Our numerical results show that the permeability for the in-line arrangement of cylinders is given by

$$K = 0.0602\varepsilon^{5.1} l^2$$

$$= 0.0602 \frac{\varepsilon^{5.1}}{(1-\varepsilon)} \frac{\pi}{4} a^2 \quad 0.40 \leqslant \varepsilon \leqslant 0.8 \tag{28}$$

e.g. for $\varepsilon = 0.5$, we have $K^{1/2} = 0.0525d$. Note that in practice, for small d, the accurate (to within $K^{1/2}$) determination of the interfacial position is difficult. We now use the numerical simulation to examine the dependence of α on the uncertainty in the assignment of the interfacial location.

Using the numerical results for the area averaged velocity $\langle u \rangle_A$, the slip coefficient evaluated at an interfacial position y_i (measured from the nominal interface) is determined from equation (3), i.e.

$$\alpha = \frac{\mathrm{d}\langle u \rangle_A}{\mathrm{d}y} \frac{K^{1/2}}{\langle u \rangle_{A,i} - u_D}. \qquad (29)$$

Figure 3(a) shows the variation of α with respect to y_i. The results show that for a change in the selected interfacial location from $y_i/l = 0$ to 0.04 ($y_i/d = 0.05$), the distance corresponding to $K^{1/2}$, the slip coefficient drops more than 50%. Saffman predicted that the inverse of α is linear with respect to y_i, i.e.

$$\frac{1}{\alpha} = C + \frac{y_i}{K^{1/2}}. \qquad (30)$$

This is also plotted in Fig. 3(a), where C is the inverse of the slip coefficient determined from the numerical results at the nominal interface. The prediction of Saffman is in excellent agreement with the present numerical results. The variation of the slip coefficient with respect to y_i is not well behaved for $y_i/l < 0$. This is because just below the nominal interface, separation of the flow occurs and wakes are formed. This is shown in Figs. 2(a) and (b), where the recirculation region is especially evident for the staggered arrangement.

The slip coefficient computed from the point solution is used in the one-dimensional solution of velocity given by equation (6). This velocity distribution is compared with the area averaged solution (obtained from the point solution) in order to examine the accuracy of the slip boundary condition and the effect of the interfacial location. As shown in Fig. 3(b), the one-dimensional solution using the slip coefficient corresponding to $y_i = -0.1l$ predicts higher mass flow rates in the channel than the area averaged solution. However, the one-dimensional solution with α evaluated at the nominal interface shows excellent agreement with the area averaged solution. This agreement is good even near the interface, where the boundary layer effects are expected to be important. As an example, the slip velocity evaluated using equation (7) is within 7% of the one from the area averaged solution. This error in velocity is much smaller for points away from the boundary. The error in the mass flow rate through the channel computed using equation (8) is less than 1% when compared to the area averaged solution.

The assumption of one-dimensional flow (Poiseuille flow) given by equation (4) does not hold at the interface because of the presence of the inertial and two-dimensional effects. These effects are easily detected from the behavior of the velocity gradient adjacent to the interface, as shown in Fig. 3(c). In this figure, the velocity gradient near the interface, normalized with respect to its values at the nominal interface, is presented for two different Reynolds numbers ($Re_l = 0.01$ and 30). For the Poiseuille flow, the velocity gradient in the channel is linear, whereas near the interface, this linearity ceases to exist due to the inertial effects as shown for $Re_l = 30$.

In order to obtain a better agreement with the Poiseuille flow in the channel, the slip coefficient can be
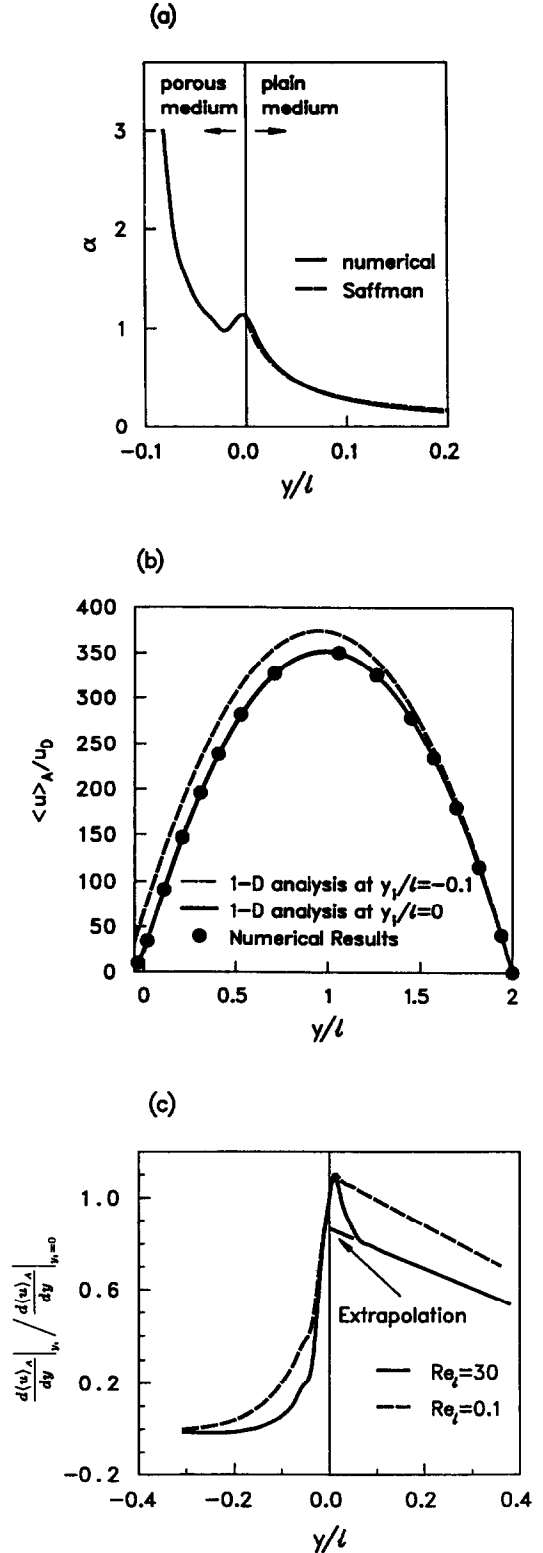

FIG. 3. (a) Variation of the slip coefficient with respect to interfacial location from the present numerical solution and the prediction of Saffman, (b) distribution of the normalized velocity in the plain medium, obtained numerically (point solution), and by the one-dimensional analysis using different interfacial locations, and (c) distribution of the shear stress normalized with respect to its value at the nominal interface, for two Reynolds numbers, showing the inertial and the two-dimensionality effects.

determined by imposing a linear variation of the velocity gradient at the interface. As shown in Fig. 3(c), this is achieved by extrapolation from a point in the channel. In the numerical experiments, this extrapolation point is generally found to be located around a distance of $0.1l$, where the boundary layer effects do not penetrate further. In order to be consistent with this velocity gradient, the slip velocity is also extrapolated from the same point. For the Poiseuille flows, the equation for the velocity is a second degree polynomial with three coefficients that could be found using the velocity gradient and the velocity at the same point in the channel, and the extrapolated gradient at the interface. Then, the interfacial velocity is evaluated with this second-order polynomial. Using α calculated with this approach, the slip velocity predicted using equation (7) is within 3% of the extrapolated one.

4.2. Inertial effects

It is generally believed that the slip coefficient depends only on the surface and bulk structural properties of the porous medium. However, we expect α to change as different flow regimes are encountered. Here, we only consider steady-state, laminar flows. The flow at the interface changes due to the inertial effects as the Reynolds number (based on flow in the porous medium) increases. These inertial effects on the velocity gradient at the interface are clearly shown in Fig. 3(c) for $Re_l = 30$. Figure 4(a) shows the variation of α with respect to the Reynolds number. For small Reynolds numbers, the viscous forces dominate and α remains constant (the flow field at the interface is invariant). For Reynolds numbers larger than 0.1, the inertial forces at the interface become significant, and the slip coefficient increases. Our numerical experiments show that for a unit cell located away from the interface (bulk behavior), the inertial effects begin to be important at a Reynolds number of about 3. The slip coefficient begins to decrease for Reynolds numbers larger than 10 because of the extrapolated shear at the interface. As shown in Fig. 3(c), for high Reynolds numbers the extrapolated velocity gradient underestimates the actual gradient, which results in a decrease in the slip coefficient. The slip coefficient without extrapolation increases monotonically for the range of Reynolds numbers shown in Fig. 4(a).

The inertial effects causing flow separations at the interface are clearly shown in Figs. 4(b) and (c), where the constant stream function contours are presented for $Re_l = 0.01$ and 30. For high Reynolds numbers, separation of the flow from the cylinder occurs closer to the top of the cylinder making the recirculation region larger, as shown in Figs. 4(b) and (c). For the low Reynolds numbers, the separation of the flow from the cylinder occurs further down on the cylinder surface. Because of these larger recirculation regions for high Reynolds numbers, the flow below the nominal interface and the slip velocity are both smaller. The difference in the interfacial velocity (normalized with the Darcean velocity) is about 20% between the
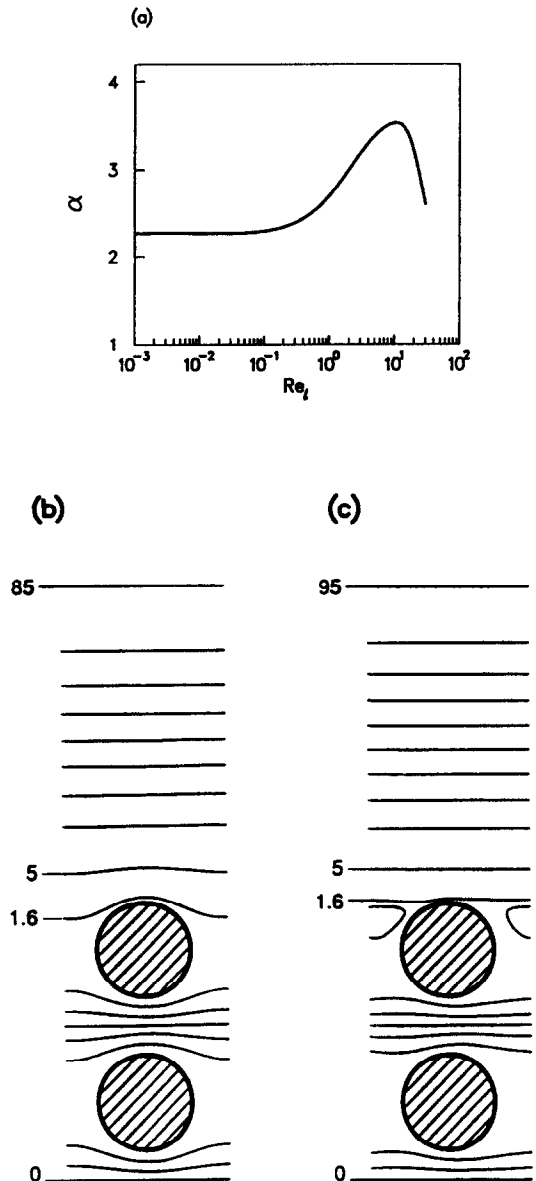

Fig. 4. (a) Variation of the slip coefficient with respect to the particle Reynolds number, (b) and (c) inertial effects at the interface are demonstrated by stream function contours for $Re_l = 0.01$ ($\psi = 0$–1.6 ($\Delta\psi = 0.2$); 5–85 ($\Delta\psi = 10$)) and 30 ($\psi = 0$–1.6 ($\Delta\psi = 0.2$); 5–95 ($\Delta\psi = 100$)), respectively.

Reynolds number of 0.01 and 30. In addition to this decrease in the velocity, there is also an increase in the shear stress due to the inertial forces. All these effects combine to give a significant difference in α as the flow changes from viscous to inertial. These inertial effects have also been reported in the numerical study [21] where gradient destruction in flow through a periodic structure was considered.

4.3. Parallel flows

The interfacial flow also changes for the different flow types (Poiseuille, Couette, or oblique) that can
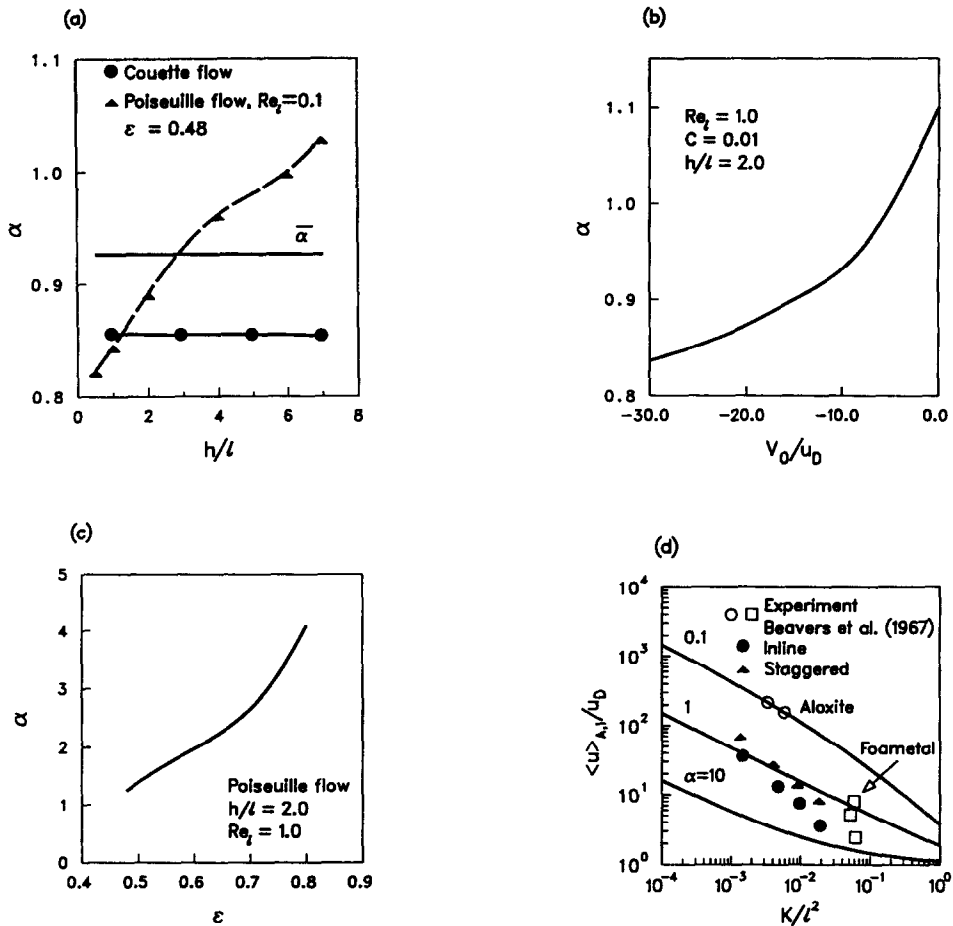
FIG. 5. (a) Variation of α with respect to the gap size for two parallel flows, Poiseuille and Couette flows, (b) variation of the slip coefficient with respect to the blowing velocity at the impermeable boundary of the channel, (c) porosity dependence of the slip coefficient for the in-line arrangement, and (d) interfacial velocity for bed of cylinders, and for real porous media, for the Poiseuille flow in a channel ($h = 3.0$).

be present in the plain layer. In this section, we study the effect of the two parallel flow types, without introducing the two-dimensional effects (i.e. oblique flows). The Couette flow condition is similar to the experiment and analysis in refs. [6, 7] and to the shear flow over a bed of cylinders [8, 9].

The numerical results show that α depends on the type of flow considered, as shown in Fig. 5(a). This is due to the inertial effects present at the interface for the Poiseuille flow. The effect of increasing the gap size, for the Poiseuille flow, is very similar to that of increasing the particle Reynolds number. As the gap size is increased, the velocity at the interface increases, and the inertial effects become important, as observed with an increase in the Reynolds number (Figs. 4(b) and (c)). This is shown in Fig. 5(a), where α increases as the gap size increases. For the Couette flow, the slip coefficient is independent of the gap size due to the absence of these inertial effects. This agrees with the experimental results in ref. [6] for flow over a grooved plate. According to Fig. 5(a), the assumption

that α is the same for the two flow types is correct when the channel dimension is between one and two cell sizes. As the gap size increases, the effect of the inertial forces becomes more pronounced and the difference in the slip coefficient between the two flows becomes larger.

When Beavers et al. performed their experiments, the slip coefficient was computed for different gap sizes using equation (8). From these different values of the slip coefficient, they computed the average value for the specimen considered. In Fig. 5(a), the average slip coefficient $\bar{\alpha}$ is given for the in-line arrangement of cylinders, as it would be found by the procedure used by Beavers et al. For the porous medium made of cylinders with slip coefficient presented in Fig. 5(a), the mass flow through the channel was computed for gap size $h/l = 0.5$ ($\sigma = 13.5$) using the slip coefficient at $h/l = 0.5$. The mass flow was also computed using the average slip coefficient $\bar{\alpha}$. The difference obtained between the two values is about 1%. Thus the averaging procedure used for the different

gap sizes gives an error well within the experimental uncertainties.

4.4. Oblique flows

All the available experimental results for the slip coefficient are based on parallel flows. This is because experiments with oblique flows are more difficult and because the relationship between the mass flow rate, α, and the gap size can be found in a closed form, as given by equation (8). The two-dimensional effects are examined here for an oblique flow with an imposed constant pressure gradient along the channel, a blowing velocity V_0 at the upper boundary, and a suction velocity CV_0 at the lower boundary. Figure 5(b) shows the variation of α with respect to the blowing velocity V_0. The slip coefficient decreases as the flow deviates from the Poiseuille flow ($V_0 = 0$), and a 24% difference is attained for $V_0/u_D = -30$. This is due to the fact that the flow is two-dimensional, whereas the Beavers and Joseph boundary condition treats the flow as one-dimensional. To account for the two-dimensional effects, the addition of another term to the slip boundary condition was suggested [22] giving an expression that is similar to the balance of the shear stress (instead of the velocity gradient across the interface). This is

$$\left.\frac{\partial\langle u\rangle_A}{\partial y}\right|_{y_1^+} + \left.\frac{\partial\langle v\rangle_A}{\partial x}\right|_{x_1} = \frac{\alpha}{K^{1/2}}(\langle u\rangle_{A,1}-u_D) \quad \text{at} \quad y_1.$$

$$(31)$$

When considering a single cell, as shown in Fig. 2(c), the $\partial\langle u\rangle_A/\partial x$ term in equation (31) is zero due to the periodicity of v. In order to assess the effect of $\partial\langle v\rangle_A/\partial x$, we examined a model with two interfacial cells laid side by side. Also, the constant blowing velocity at the upper boundary giving a periodic flow in each cell was replaced by a blowing velocity that varies linearly with x. These calculations have shown that the difference in the calculated α is less than 1%, when the second term is included. Thus, we conclude that the second term would not account for the two-dimensional effects, since its contribution is not significant. Generally, the first term is much larger than the second one, since the averaged velocity across the interface varies more significantly than that along the interface. These same observations were made in ref. [23] when the two-dimensional boundary condition was used to analyze the liquid droplet levitation on a heated porous layer. It was found that the second term did not noticeably change the levitation distance (gap size) predictions.

4.5. Porosity

In the experiments conducted by Beavers et al. [1, 3, 4], the slip coefficient was evaluated for a wide range of permeabilities spanning over two orders of magnitude. Over this range of permeability, α decreased monotonically as the permeability decreased. This suggests that α has a very strong

dependence on the permeability and the porosity. This strong dependence is also observed for the periodic structure considered here. The slip coefficient computed for a given Reynolds number and gap size is shown as a function of porosity in Fig. 5(c). As expected, when the porosity increases, the slip coefficient increases showing agreement with the few experimental data for random (disordered) porous media.

In order to evaluate the present model and the disordered porous media, we have calculated the slip velocity for the in-line and for the staggered arrangements of cylinders and compared it to the data provided in ref. [1]. The cell size l used to non-dimensionalize their permeability is based on their reported pore size. The slip velocity for the Poiseuille flow, in terms of the Darcean velocity, is obtained by combining equations (1) for one-dimensional flow and equation (7), which gives

$$\langle u\rangle_{A,1} = \frac{u_D}{2}\frac{\sigma^2+2\alpha\sigma}{1+\alpha\sigma}. \qquad (32)$$

The results for the slip velocity are presented in Fig. 5(d) as a function of normalized permeability. Unfortunately, not enough experimental data are available to give a thorough comparison between the two media. However, comparison with the limited available experimental results show that the slip velocity predicted for the two-dimensional periodic structures, are within those measured for the disordered porous media.

4.6. Surface structure

When Beavers and Joseph suggested the slip boundary condition, they suggested that the slip coefficient would be strongly dependent on the surface structure of the porous medium. Later, Beavers et al. [4] found that α changed by 85% after they machined the surface of the porous slab. In the present model, it is possible to study the surface nonuniformities by using different arrangements of the interfacial row of cylinders. For this purpose, we have taken a surface structure for an in-line arrangement of cylinders, as depicted by Fig. 6(a), where the variable distance λ represents the surface nonuniformity (e.g. particle dislocation). In random porous media, λ would represent the surface roughness (beyond the nominal surface). The variation of the slip coefficient is shown in Fig. 6(b) as the distance λ is varied between 0 and $l/2$. For a non-zero offset, the fluid flow at the nominal interface increases giving rise to a higher slip velocity. Therefore, the slip coefficient decreases significantly as the offset increases.

The slip coefficient is also calculated for a staggered arrangement of cylinders. In this configuration every column of cylinders is offset with respect to the neighboring ones by $l/2$, as shown in Fig. 2(a). When the slip coefficient for the staggered arrangement is compared to the one for the in-line arrangement for an
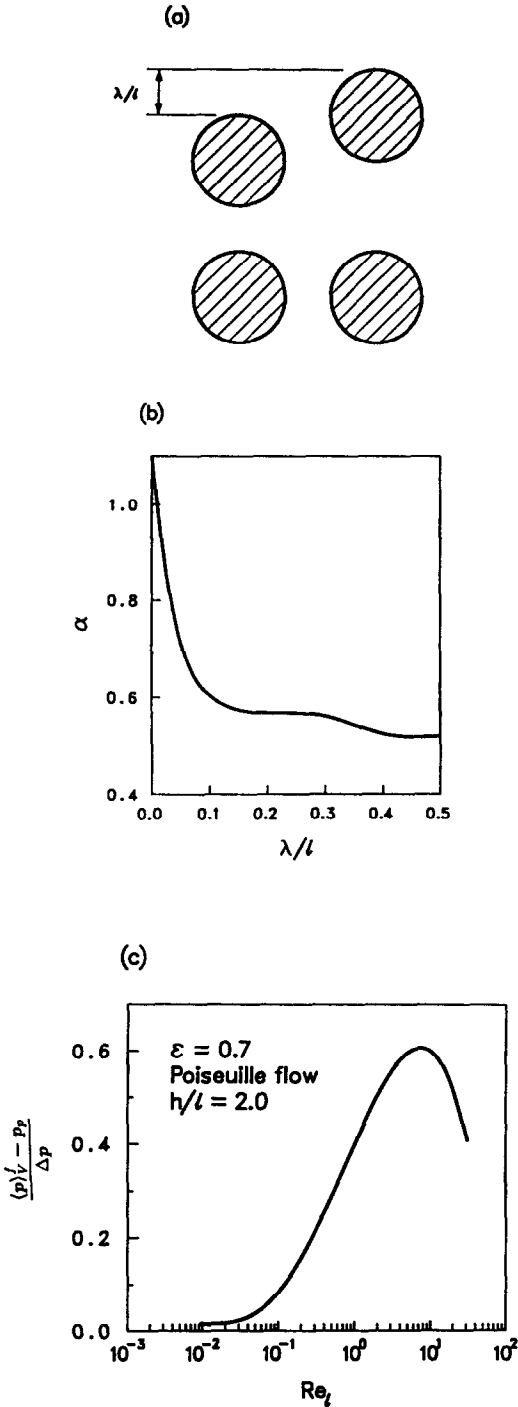
(a)

(b)

(c)

FIG. 6. (a) The interfacial arrangement representing surface nonuniformity, (b) variation of α with respect to the offset λ, and (c) pressure slip variation with respect to the Reynolds number for an in-line arrangement.

offset distance $\lambda = l/2$, a 2% difference is obtained. This shows that α is mainly a surface property, because the two configurations have the same surface structure but the bulk structures are different. Note that the difference in the permeability for the two cylinder arrangements (for $\varepsilon = 0.48$) is about 10%.

4.7. Pressure slip

In the previous sections, we have discussed the velocity slip that occurs at the interface of a porous and a plain medium. The slip is due to the averaging performed in order to obtain the Darcean flow in the porous medium. A pressure slip also occurs, when the pressure is averaged in the porous medium. This pressure slip has been investigated in ref. [24] using an order of magnitude analysis for low Reynolds number flow in a periodic structure. Through this analysis, it was found that the pressure jump across the interface, for parallel flow is comparable to the pressure difference across the cell, i.e.

$$\frac{\langle p \rangle_{V}^{f} - p_{p}}{l} = O\left(\frac{\Delta p}{l}\right) \tag{33}$$

where p_{p} is the average pressure in the plain medium over the cell length.

Our interfacial simulation allows for the study of the pressure slip and verification of equation (33). The point solution to the pressure field reveals that this pressure jump is mainly induced by the inertial effects present at the interface at high Re_{l}. This is clearly shown in Fig. 6(c) where the pressure slip, normalized by the pressure difference across the unit cell, is given as a function of Re_{l}. For low Reynolds numbers (< 0.3), the flow at the interface is Stokean and symmetric with respect to the cylinder axis, as shown in Fig. 4(b). Due to this symmetry, the point pressure gradient in the y-direction varies spatially as an odd function of y (with respect to the same axis). Thus, when the pressure is averaged in the x-direction (area averaged $\langle p \rangle_{A}$), the resulting pressure difference across the interface (pressure slip) in the y-direction is negligible. From Fig. 6(c), we observe that the pressure slip is very small compared to the pressure difference across the cell and can be neglected. This result is in contradiction with the results from ref. [24] due to the approximate nature of the analysis. For higher Reynolds numbers, inertial effects are more important, and as expected, the flow is not symmetric because of the flow separation, as shown by Fig. 4(c). Inherent in the non-symmetric behavior of the velocity field, the variation of the point pressure gradient in the y-direction does not follow that of an odd function at the interface. Hence, when averaging of the pressure in the x-direction is performed, a pressure difference across the interface (in the y-direction) is found. For high Reynolds numbers, this pressure difference is of the same order as the pressure difference across the cell.

As with the velocity slip coefficient, the pressure slip was also examined with the presence of surface non-uniformities. It was found that the pressure slip does not vary significantly when the offset λ is increased. For all practical purposes, the pressure slip across the interface is negligible on the macro-scale where the pressure drop across the porous medium increases with the number of cells.

5. RESULTS FOR NO-SLIP CONDITION

When the no-slip boundary condition is used, special attention should be given to the choice of the averaging volume. The averaging volume must be small enough so that the velocity variations near the interface are not masked. Moreover, the averaging volume should be taken in such a way that the interfacial velocity (as obtained from the local simulation) and the Darcean velocity (in the bulk of the porous medium) are recovered. If a unit cell is taken as the averaging volume, it will mask the velocity variation over the Brinkman screening distance. The numerical results show that for the range of porosities considered, the bulk flow is recovered at the lower half of the interfacial row of cylinders. Thus the volume averaged velocity should not make this boundary layer effect penetrate beyond one cell into the porous medium.

Based on these, we choose an averaging volume that has an infinitesimal thickness at the interface (guaranteeing the no-slip condition). For points away from the interface, the averaging volume increases with the distance from the interface (to a cell size) so that the Darcean velocity is recovered. In the numerical computations, the averaging volume is the grid size, at the nominal interface, and the cell size at $y \leqslant -l/2$. For any point y existing between 0 and $-l/2$ the averaging volume is taken as $-2yl$, and the volume averaged velocity is defined as

$$\langle u \rangle_V(y) \equiv \frac{-1}{2yl} \int_{-2y}^{0} \int_{0}^{l} u(x, y') \, \mathrm{d}x \, \mathrm{d}y'. \quad (34)$$

Using this volume averaging procedure, the three no-slip models (equations (12)–(14)) are examined below.

5.1. Brinkman model

This Brinkman model is commonly used in the analysis of flow and heat transfer in composite (porous-plain) media. Some investigators have added, in an ad hoc manner, a macroscopic shear term to the Darcy law (with $\mu' = \mu$) to allow for the variation of the velocity near the boundary. Others, e.g. Lundgren [25], have formally proved the validity of the Brinkman equation for dilute concentration of particles. In applying equation (12), the viscosity μ' needs to be prescribed. Brinkman suggested $\mu' = \mu$, while later Lundgren showed that $\mu' = \mu(\mu', \varepsilon)$.

Here, the results of the one-dimensional Brinkman model are compared to the volume averaged, point solution (direct simulation) in an attempt to examine the validity of this model. We begin by using the result for a parallel flow from ref. [10], which gives $\mu'/\mu = \alpha^2$. Therefore, we guarantee that the interface velocity obtained from the Brinkman equation is the same as that obtained from the local simulation (within a small error). The boundary conditions used here are similar to the Beavers and Joseph model discussed earlier,

except at the interface where the continuity conditions are used, i.e.

$$u(0) = \langle u \rangle_V(0) \quad \text{and} \quad \mu \frac{\mathrm{d}u}{\mathrm{d}y}\bigg|_{0^+} = \mu' \frac{\mathrm{d}\langle u \rangle_V}{\mathrm{d}y}\bigg|_{0^-}. \quad (35)$$

The solution obtained in the plain medium is given by equation (6) (using $\mu'/\mu = \alpha^2$) and in the porous medium the velocity distribution is [10]

$$\langle u \rangle_V(y) = -\frac{K}{\mu} \frac{\mathrm{d}p}{\mathrm{d}x} \left[1 + \frac{\sigma^2 - 2}{2(1 + \sigma\alpha)} \exp\left(\frac{1}{\alpha} \frac{y}{\sqrt{k}}\right) \right]. \quad (36)$$

This velocity profile is presented in Fig. 7(a) and compared with the volume averaged point solution. These results show that the volume (given by equation (34)) and area averaged solutions reach the bulk behavior within the interfacial cell, whereas the Brinkman model reaches the bulk behavior beyond the second cell. The Brinkman model, using a small decay factor in equation (36), underestimates the resistance to the flow at the interface and makes the boundary effect penetrate further into the porous medium. The resistance at the interface is also underestimated using boundary conditions (35) which establish continuity of the shear stress at the interface. For $\varepsilon = 0.8$, we have $\mu'/\mu \approx 16$, which gives a small velocity gradient at the interface (on the porous medium side). This smaller velocity gradient makes the boundary effect penetrate more into the porous medium (compared to the averaged solution). Note that the screening length is $K^{1/2} = 0.267d$ (for $\varepsilon = 0.8$). The Brinkman model results in a velocity profile that is much closer to the local simulation for $\varepsilon = 0.48$, where the ratio of the viscosities is very close to unity. However, for a staggered cylinder arrangement, as shown in Fig. 2(a), the Brinkman model gives a faster decay than the point solution. Thus, we conclude that the Brinkman model with a constant effective viscosity predicts the right slip velocity but generally does not result in the correct profile in the porous medium near the interface. This shortcoming might be overcome by using a variable effective viscosity model, as discussed below.

5.2. Variable effective viscosity model

In the variable effective viscosity model, $\mu'(y)$ is readily obtained by using the volume averaged point distribution by integration of equation (13), i.e.

$$\mu'(y) = \frac{\int_{0}^{y} \left[\frac{\mathrm{d}\langle p \rangle_V^l}{\mathrm{d}x} + \frac{\mu}{K} \langle u \rangle_V(y') \right] \mathrm{d}y' + \mu'(0) \frac{\mathrm{d}\langle u \rangle_V}{\mathrm{d}y}\bigg|_{0}}{\frac{\mathrm{d}\langle u \rangle_V}{\mathrm{d}y}\bigg|_{y}} \quad (37)$$

where $\mu'(0)$ is taken as the fluid viscosity μ, which will give a continuous velocity gradient on both sides of the interface as the boundary condition. In Fig. 7(b),
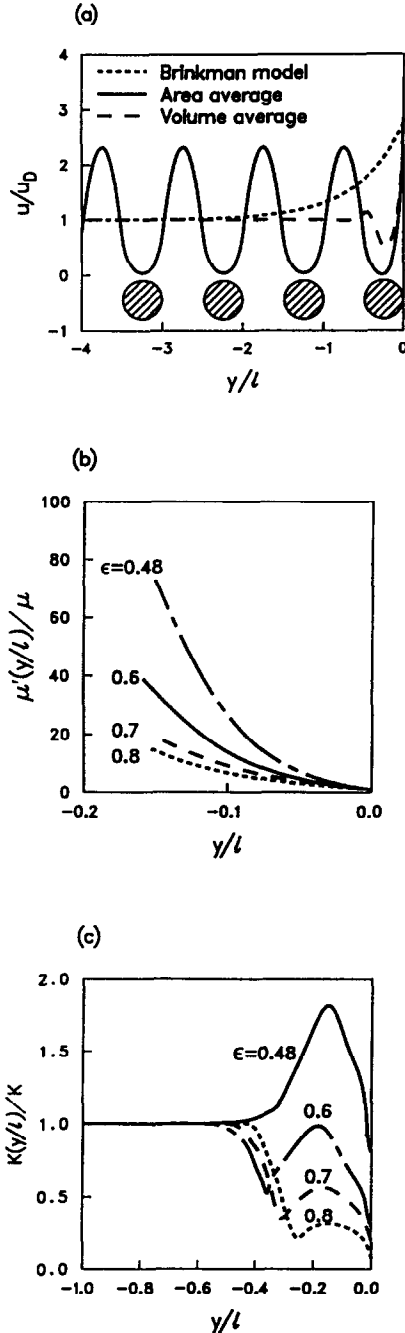
(a)

(b)

(c)

Fig. 7. (a) Comparison of the velocity distribution obtained from the Brinkman solution, the area averaged local solution, and the volume (variable volume) averaged local solution using $\langle u \rangle_V(y) = (-1/2yl)\int_{-2y}^{0} \int_{0}^{l} u(x, y')\,dx\,dy'$, (b) local effective viscosity distribution, and (c) local permeability distribution. Both (b) and (c) are for the in-line arrangement of cylinders with different porosities.

the ratio of the local effective to the fluid viscosity is given as a function of y/l. The results are only for $y/l > -0.2$, because further into the porous medium $d\langle u \rangle_V/dy \to 0$ and $\mu'(y)$ is undetermined (large oscillations of μ' occur). The local effective viscosity, as

shown in Fig. 7(b), decreases with an increase in porosity, because the pore size becomes larger and the fluid encounters less resistance.

The variation of the effective viscosity found above for $\varepsilon = 0.8$ is used in equation (13) in order to examine the accuracy of the predicted velocity distribution near the interface. A fifth degree polynomial is used for μ', which ignores the large oscillations and allows for an asymptotic, very large value of μ' away from the interface (because of the very small denominator in equation (37)). An upper bound is prescribed for μ'/μ, and it is found that by changing this bound from 10^4 to 10^7, the interfacial velocity changes only by 1%. For the condition used in Fig. 7(b) and $\varepsilon = 0.8$, this variable effective viscosity model is compared with the point solution. The model predicts the penetration depth and the velocity gradient very well. However, the predicted slip velocity is 37% (higher) than that of the point solution. The error in the mass flow rate through the channel is about 3% (higher).

The effect of the surface nonuniformity on the local effective viscosity was also examined in the same manner as for the slip coefficient. Since the local effective viscosity depends on the local geometry, it is expected to change with the surface structure. As the offset λ between the cylinders of the interfacial row increases, the flow below the interface increases (because of the lower resistance). Thus, the effective viscosity decreases as the offset λ increases.

5.3. Variable permeability model

This model has been used previously to study the flow and heat transfer in porous media near bounding, impermeable surfaces. Commonly, an area averaged void distribution $\varepsilon(y)$ is prescribed based on the experimental results for random packing of spheres. Then, the permeability is calculated using the Carman–Kozeny relation. Here, as was done above for the variable effective viscosity model, we find the variation in the permeability near the interface from the computed velocity field and by using equation (14), i.e.

$$K(y) = \frac{\mu\langle u \rangle_V}{\mu\dfrac{d^2\langle u \rangle_V}{dy^2} - \dfrac{d\langle p \rangle_V^i}{dx}}. \qquad (38)$$

The computed variation of the permeability near the interface is shown in Fig. 7(c) for the in-line arrangement for various porosities. Intuitively, we expect the permeability to be higher at the interface, because of the lower resistance to the flow (compared to the bulk permeability). However, the results show that the surface permeability is lower than that in the bulk, except for $\varepsilon = 0.48$. This decrease in the permeability is due to the dominating effect of the shear stress term in equation (14). From these results, we infer that the permeability at the interface cannot be modeled using $\varepsilon(y)$ and the Carman–Kozeny relation.

The variable permeability found above for $\varepsilon = 0.8$ is

used in equation (14) in order to examine the predicted velocity near the interface. Since the local permeability does not diverge for points away from the interface, the discrete values of the permeability as calculated by equation (38) are used. The error in the interface velocity is about 24% (higher), and the error in the mass flow through the channel is about 2% (higher).

As with the slip coefficient, the effect of the surface nonuniformity on the local permeability is also examined for the in-line arrangement. As the offset distance λ is increased, the local permeability increases (because of the lower resistance), showing the dependence of $K(y)$ on the surface structure.

6. CONCLUSIONS

By direct simulation of the flow at and near the porous, plain media interface, we have examined the dependence of the slip coefficient in the boundary condition commonly used at this interface. We have found that

$$\alpha = \alpha(\varepsilon, Re_l, h, y_i, \text{bulk flow direction,}$$
$$\text{and surface structure}). \quad (39)$$

We have found that the most appropriate choice for the interfacial location is the nominal interface (i.e. the top of the interfacial cylinders). We also point to the sensitivity of α on the choice of y_i and conclude that since, in actual surfaces, the measurement of h (or y_i) involves uncertainties of the order of the Brinkman screening distance $K^{1/2}$, and since α changes noticeably over $y_i = O(K^{1/2})$ the experimentally determined values of α will be apparatus dependent.

The pressure slip across the interface has been examined and at low Reynolds numbers ($Re_l \leqslant 0.1$), this pressure slip is very small when compared to the pressure drop across a unit cell. At higher Reynolds numbers, the pressure slip is of the same order of magnitude as the pressure drop across a unit cell.

By examining the Brinkman treatment of the interfacial hydrodynamics, we have found that $\mu'(y)$ and $K(y)$ cannot be given in general forms.

We plan to continue the examination of the validity of the one-dimensional treatments by considering heat transfer across and along the interface. There, the temperature slip will depend on the interfacial hydrodynamic approximation discussed here.

REFERENCES

1. G. S. Beavers and D. D. Joseph, Boundary conditions at a naturally permeable wall, *J. Fluid Mech.* **30**, 197–207 (1967).
2. H. C. Brinkman, A calculation of the viscous force exerted by a flowing fluid on a dense swarm of particles, *Appl. Scient. Res.* **A1**, 27–34 (1947).
3. G. S. Beavers, E. M. Sparrow and R. A. Magnuson, Experiments on coupled parallel flows in a channel and a bounding porous medium, *J. Basic Engng* **92D**, 843–848 (1970).
4. G. S. Beavers, E. M. Sparrow and B. A. Masha, Boundary condition at a porous surface which bounds a fluid flow, *A.I.Ch.E. Jl* **20**, 596–597 (1974).
5. P. G. Saffman, On the boundary condition at the surface of a porous medium, *Stud. Appl. Math.* **L**, 93–101 (1971).
6. G. I. Taylor, A model for the boundary condition of a porous material, Part 1, *J. Fluid. Mech.* **49**, 319–326 (1971).
7. S. A. Richardson, A model for the boundary condition of a porous material, Part 2, *J. Fluid. Mech.* **49**, 327–336 (1971).
8. R. E. Larson and J. J. L. Higdon, Microscopic flow near the surface of two-dimensional porous media, Part 1 : axial flow, *J. Fluid Mech.* **166**, 449–472 (1986).
9. R. E. Larson and J. J. L. Higdon, Microscopic flow near the surface of two-dimensional porous media, Part 2 : transverse flow, *J. Fluid. Mech.* **178**, 119–136 (1987).
10. G. Neale and W. Nader, Practical significance of Brinkman's extension of Darcy's law : coupled parallel flows within a channel and a bounding porous medium, *Can. J. Chem. Engng* **52**, 475–478 (1974).
11. K. Vafai and R. Thiyagaraja, Analysis of flow and heat transfer at the interface region of a porous medium, *Int. J. Heat Mass Transfer* **30**, 1391–1405 (1987).
12. K. Vafai, Convective flow and heat transfer invariable-porosity media, *J. Fluid. Mech.* **147**, 233–259 (1984).
13. P. Cheng and D. Vortmeyer, Transverse thermal dispersion and wall channelling in a packed bed with forced convective flow, *Chem. Engng Sci.* **43**, 2523–2532 (1988).
14. A. S. Sangani and S. Behl, The planar singular solutions of Stokes and Laplace equations and their application to transport processes near porous surfaces, *Physics Fluids* **A1**, 21–37 (1989).
15. M. Kaviany, *Principles of Heat Transfer in Porous Media*, Mechanical Engineering Series. Springer, New York (1991).
16. B. E. Launder and T. H. Massey, The numerical prediction of viscous flow and heat transfer in tube banks, *ASME J. Heat Transfer* **100**, 565–571 (1978).
17. H. T. Prata and E. M. Sparrow, Forced convection evaporation from a cavity containing a liquid whose surface is curved by capillarity : computations in interlocking rectangular and cylindrical domains, *Numer. Heat Transfer* **12**, 667–688 (1985).
18. S. V. Patankar, *Numerical Heat Transfer and Fluid Flow*. Hemisphere, Washington, DC (1980).
19. O. P. Bergelin, A. P. Colburn and L. H. Hall, Bulletin No. 2 University of Delaware Engng Exp. Station (1950).
20. D. A. Edwards, M. Shapiro, P. Bar-Yoseph and M. Shapira, The influence of Reynolds number upon the apparent permeability on spatially periodic arrays of cylinders, *Physics Fluids* **A2**, 45–55 (1989).
21. M. Kaviany, Gradient destruction in flow through a rigid matrix, *J. Fluid Mech.* **165**, 221–230 (1986).
22. I. P. Jones, Low Reynolds number flow past a porous spherical shell, *Proc. Camb. Phil. Soc.* **73**, 231–238 (1973).
23. M. Fatehi and M. Kaviany, Analysis of levitation of saturated liquid droplets on permeable surfaces, *Int. J. Heat Mass Transfer* **33**, 983–994 (1990).
24. H. I. Ene and E. Sanchez-Palencia, Equation et phenomene de surface pour l'écoulement dans un modele de milieu poreux, *J. Mecanique* **14**, 73–107 (1975).
25. T. S. Lundgren, Slow flow through stationary random beds and suspensions of spheres, *J. Fluid Mech.* **51**, 273–299 (1972).

CONDITIONS AUX LIMITES DE VITESSE AVEC OU SANS GLISSEMENT A L'INTERFACE DES MILIEUX POREUX ET COMPACT

Résumé—La condition hydrodynamique à l'interface entre un milieu poreux et un milieu compact est examinée par une simulation directe du champ d'écoulement bidimensionnel près de l'interface d'un milieu poreux fait de cylindres. On examine la condition de glissement qui contient un coefficient de glissement α et celle de non glissement qui contient une viscosité effective μ'. On examine en détail la dépendance de α et de la direction de l'écoulement (par rapport au plan de l'interface), la porosité, le nombre de Reynolds (basé sur la longueur de la cellule et la vitesse darcienne), la sélection de la localisation interfaciale et l'arrangement des cylindres (structure). Les résultats numériques montrent que α n'est pas seulement fonction de la structure mais qu'il dépend de la direction de l'écoulement, du nombre de Reynolds, de l'étendue du milieu compact et des changements de l'arrangement des particules à la surface. On montre aussi que pour une prévision précise de la vitesse locale près de l'interface (dans le milieu poreux) μ' doit varier dans le milieu poreux. Ceci montre que l'extension de Brinkman basée sur μ' uniforme et la distance associée ne modélisent pas de façon satisfaisante le champ d'écoulement dans le milieu poreux.

GESCHWINDIGKEITSRANDBEDINGUNGEN AN DER GRENZFLÄCHE PORÖSER EBENER MEDIEN MIT UND OHNE SCHLUPF

Zusammenfassung—Die hydrodynamische Randbedingung an der Grenzfläche zwischen einem porösen und einem glatten Medium wird durch direkte Simulation des zweidimensionalen Strömungsfeldes nahe der Oberfläche eines porösen Zylinders untersucht. Es wird eine Randbedingung mit Schlupf, gekennzeichnet durch einen Gleitkoeffizienten α, und eine ohne Schlupf betrachtet, die eine effektive Viskosität μ' enthält. Die Abhängigkeit des Begleitkoeffizienten α von der Strömungsrichtung (bezogen auf die Grenzfläche), der Porosität, der Reynolds-Zahl (gebildet mit der Länge der Einheitszelle und der Darcy-Geschwindigkeit), der Wahl des Ortes an der Grenzfläche und der Anordnung der Zylinder (Struktur) wird im einzelnen untersucht. Die numerischen Ergebnisse zeigen, daß α nicht nur eine Funktion der Struktur ist, sondern auch von der Strömungsrichtung, der Reynolds-Zahl, der Ausdehnung des glatten Mediums sowie den Ungleichförmigkeiten bei der Anordnung der Oberflächenpartikel abhängt. Es zeigt sich auch, daß für eine genaue Vorausberechnung der örtlichen Geschwindigkeit nahe der Grenzfläche (im Inneren des porösen Mediums) μ' innerhalb des porösen Mediums variieren muß. Daraus ergibt sich, daß mit Hilfe der Formulierung nach Brinkman auf der Grundlage einer gleichförmigen effektiven Viskosität μ' und dem damit verbundenen Gitterabstand das Strömungsfeld innerhalb des porösen Mediums nicht befriedigend modelliert werden kann.

ГРАНИЧНЫЕ УСЛОВИЯ ПРИ НАЛИЧИИ И ОТСУТСТВИИ СКОЛЬЖЕНИЯ НА ГРАНИЦЕ РАЗДЕЛА ПОРИСТОЙ И НЕПОРИСТОЙ СРЕД

Аннотация—С использованием прямого моделирования двумерного поля течения вблизи границы раздела пористой среды, содержащей цилиндрические каналы, и обычной (непористой) среды исследуется гидродинамическое граничное условие на границе раздела этих сред. Рассматриваются граничное условие со скольжением, содержащее коэффициент скольжения α, и граничное условие при отсутствии скольжения, включающее эффективную вязкость μ'. Детально исследуется зависимость значения α от направления течения, порозности, числа Рейнольдса (содержащего размер единичной ячейки и скорость Дарси), выбора расположения границы раздела и размещения цилиндров (структуры). Численные результаты показывают, что значение α зависит не только от структуры, но также и от направления течения, числа Рейнольдса, протяженности непористой среды. Показано также, что для точного расчета локальной скорости вблизи границы раздела (внутри пористой среды) значение μ' следует считать изменяющимся в пределах пористой среды. Это свидетельствует о том, что модель Бринкмана, основанная на постоянном значении μ' и наличии области экранирования, неудовлетворительно моделирует поле течения в пористой среде.